# **Malaysian Journal of Analytical Sciences** (MJAS) Published by Malaysian Analytical Sciences Society



# ROLE OF VANADIA AND TITANIA PHASES IN THE REMOVAL OF METHYLENE BLUE BY ADSORPTION AND PHOTOCATALYTIC **DEGRADATION**

(Peranan Fasa Vanadia dan Titania dalam Penyingkiran Metilena Biru Melalui Penjerapan dan Degradasi Fotokatalisis)

Pei Wen Koh<sup>1,2</sup>, Cheng Yee Leong<sup>2</sup>, Leny Yuliati<sup>2,3</sup>, Hadi Nur<sup>2</sup>, Siew Ling Lee<sup>2\*</sup>

<sup>1</sup>Department of Chemistry, Faculty of Science <sup>2</sup>Centre for Sustainable Nanomaterials, Ibnu Sina Institute for Scientific and Industrial Research Universiti Teknologi Malaysia, 81300 Johor Bahru, Malaysia <sup>3</sup>Ma Chung Center for Photosynthetic Pigments, Universitas Ma Chung, Malang 65151, Indonesia

\*Corresponding author: sllee@ibnusina.utm.my

Received: 18 July 2019; Accepted: 20 July 2020; Published: 10 December 2020

#### **Abstract**

Total removal of methylene blue (MB) over vanadia (V<sub>2</sub>O<sub>5</sub>) -modified titania (TiO<sub>2</sub>) composite demonstrated that the V<sub>2</sub>O<sub>5</sub> and TiO<sub>2</sub> phases played a vital role in the adsorption and photodegradation of MB, respectively. The 10 mol% of V<sub>2</sub>O<sub>5</sub>- modified TiO<sub>2</sub> (10V-TiO<sub>2</sub>) showed the highest removal of MB, i.e., 26- and 2-folds better adsorption capacity than that of undoped TiO<sub>2</sub> and V<sub>2</sub>O<sub>5</sub>, respectively. The presence of surface hydroxyl, pores, and the highest amount of V<sup>5+</sup> species in 10V-TiO<sub>2</sub> could be responsible for the high adsorption of MB. V<sub>2</sub>O<sub>5</sub> induced anatase to rutile phase transformation and shifted absorption properties of TiO<sub>2</sub> to the visible light region. Considering the rutile phase has lower bandgap energy (3.0 eV), its presence in the sample has enhanced the photodegradation of MB. The photodegradation of MB followed pseudo-second-order reaction. The reusability test elucidated that the photodegradation performance of 10V-TiO<sub>2</sub> was improved by 30-folds after the second cycle, with total MB removal due to the exposure of more TiO2 to MB.

**Keywords:** vanadia, titania, methylene blue, adsorption, photocatalyst, photodegradation

#### Abstrak

Penyingkiran metilena biru (MB) secara keseluruhan oleh komposit titania (TiO<sub>2</sub>) yang diubahsuai dengan vanadia (V<sub>2</sub>O<sub>5</sub>) menunjukkan bahawa fasa V<sub>2</sub>O<sub>5</sub> dan TiO<sub>2</sub> masing-masing memainkan peranan penting dalam penjerapan dan fotodegradasi MB. TiO<sub>2</sub> yang diubahsuai dengan 10 mol% V<sub>2</sub>O<sub>5</sub> (10V-TiO<sub>2</sub>) menunjukkan penyingkiran MB yang tertinggi, iaitu 26- dan 2-kali ganda kapasiti penjerapan yang lebih baik daripada TiO2 dan V2O5 yang tidak didopkan. Kewujudan hidrosil di permukaan, liang, dan jumlah spesis V<sup>5+</sup> tertinggi dalam 10V-TiO<sub>2</sub> menyumbang kepada penjerapan MB yang tinggi. V<sub>2</sub>O<sub>5</sub> mendorong transformasi fasa anatase ke rutil dan sifat-sifat penyerapan TiO<sub>2</sub> beralih ke rantau cahaya nampak. Memandangkan fasa rutil mempunyai tenaga jurang jalur yang lebih rendah (3.0 eV), kewujudannya dalam sampel telah meningkatkan prestasi fotodegradasi MB. Fotodegradasi MB mengikuti tindak balas tertib pseudo-kedua. Ujian kebolehgunaan tersebut membuktikan bahawa prestasi

fotodegradasi 10V-TiO<sub>2</sub> telah ditingkatkan sebanyak 30-kali ganda selepas kitaran kedua kerana lebih banyak TiO<sub>2</sub> terdedah kepada MB.

Kata kunci: vanadia, titania, metilena biru, penjerapan, fotokatalis, fotodegradasi

### Introduction

Soil and water contamination by dye-containing effluents are serious environmental issues. The release of these coloured compounds into the drainage system has significantly impacted human and aquatic lives due to their toxicity. Although many technologies have been developed to treat dye-containing effluent at an acceptable level before drainage, there is no single process capable of adequately treating these dyecontaining wastewaters. It was suggested that a combination of different techniques would be a better solution to remove the dyes [1, 2]. Compared to the conventional biological physicochemical method, it is undeniable that adsorption is a superior method established for the removal of dye due to its simplicity in design, efficiency, and ability to treat dye in larger quantities [3]. A good adsorbent should have high selectivity and adsorption capacity for the targeted adsorbate. However, in many cases, surface modification using an expensive surfactant, chemical, or heat treatment is always applied to solve the limitations of the surface functional group of adsorbents [4]. Another shortcoming of the adsorption method is associated with the formation of secondary pollution following the adsorption process. Photocatalysis appears to be a promising green technology approach to address this problem compared to conventional treatments such as flocculation, coagulation, and adsorption, which often result in secondary pollution [5, 6]. Photocatalysis is capable of fully mineralising toxic dye to non-toxic anionic compounds. However, its usage is only applicable to trace amount of dye-containing wastewater.

Among many semiconductor photocatalysts, titanium dioxide (TiO<sub>2</sub>) has gained considerable attention due to its high activity, high light-illumination stability, nontoxic properties, and low price [7]. However, its low surface area has limited its adsorption and photocatalytic

degradation efficiency under ultraviolet (UV) light. Recently, comprehensive review and studies on the effectiveness of incorporating TiO2 on porous adsorbents had been reported [8-10]. The catalytic performance of TiO<sub>2</sub> can be improved by loading TiO<sub>2</sub> onto various supporting adsorbents. Other drawbacks of TiO2 photocatalyst include high recombination rate of the electron-hole, high bandgap energy, and inactivity under visible light that affected its application under sunlight. A standard method used to solve the problems above is the modification of TiO2 via transition metal doping. Transition metal doping appears to be one of the most effective approaches to reduce the rate of electrons and holes recombination [1, 11-13]. Visible light-driven vanadia-doped titania photocatalysts in pure anatase phase have been reported [14, 15]. Their enhanced photocatalytic behaviour was attributed to the highly dispersed vanadia in the TiO2 crystallite, which successfully reduced the bandgap energy and increased the ability to absorb visible light.

Nguyen et al. reported that 10% vanadia-doped TiO<sub>2</sub> (V-TiO<sub>2</sub>) is an excellent adsorbent for decolourisation of methylene blue (MB) [16]. This material possessed anatase and a negligible percentage of brookite phases. It was claimed that the good interaction between vanadia-doped TiO2 and the dye molecules as well as the increased oxidation states of Ti, V, and O have contributed to the excellent adsorption ability of the material, resulting in the removal of 91.6% MB after 2 hours reaction time [16]. The usage of V-TiO<sub>2</sub> as a photocatalyst has been widely reported. In the current study, we present new insight into the role of the respective vanadia and titania in the V-TiO<sub>2</sub> composite through adsorption and photocatalysis of MB. MB was selected as a model reaction because it is widely used for dyeing in many industries such as silk, paper, ink and used as cotton mordant with tannin [2].

### **Materials and Methods**

### **Materials**

The materials used for this study include titanium tetraisopropoxide (TTIP; 97%, Aldrich), absolute ethanol (99.98%, HmBG), acetylacetone (≥ 99%, Aldrich), and vanadyl acetylacetonate (98%, Aldrich).

## Synthesis of vanadia modified titania

Vanadia-modified titania (V-TiO<sub>2</sub>) materials were prepared through the sol-gel method. The experimental procedures were reported in previous studies [2, 17]. In a typical synthesis, titanium tetraisopropoxide (TTIP; 97%, Aldrich) was mixed with absolute ethanol (99.98%, HmBG) and acetylacetone (≥ 99%, Aldrich) according to the molar ratio of 1:100:2. The mixture was then stirred for 60 min at room temperature. Vanadia precursor was prepared separately by dissolving a precalculated amount of vanadyl acetylacetonate (98%, Aldrich) in acetylacetone. The two solutions were mixed and stirred for 30 minutes at room temperature, followed by evaporation at 353 K. The obtained solid material was calcined at 773 K for 5 hours. The molar ratio of vanadia in TiO2 was varied from 1 to 10 mol%. The resulted materials were denoted as xV-TiO2, where x represents mol% of V. Undoped TiO<sub>2</sub> was prepared with the same procedures without the addition of vanadyl acetylacetonate for comparison. Bulk V2O5 was prepared by evaporating vanadyl acetylacetonate (98%, Aldrich) in acetylacetone at 273 K, followed by calcination at 773 K for 5 hours.

# Characterisation

Phase purity and crystallinity of the synthesised undoped  $TiO_2$ , vanadium oxide-modified titania, and bulk  $V_2O_5$  samples were examined using Powder X-ray diffraction (XRD) analyser. The XRD measurements were conducted on Bruker Advance D8 X-ray diffractometer with Cu K $\alpha$  radiation ( $\lambda$  = 0.15418 nm, 40 KV, 40 mA, scan rate 0.1°/s). The Diffuse reflectance UV-visible (DR UV-Vis) spectra were recorded on Perkin Elmer Ultraviolet-visible Spectrometer Lambda 900 with BaSO<sub>4</sub> as reference. Bandgap energy of the samples was calculated from the extrapolation of the Tauc plot. Surface morphology of the prepared samples was investigated using Field Emission Scanning Electron Microscopy (FESEM). The samples were

coated with platinum using Auto Fine Coater (JEOL JFC-1600), prior to analysis using a FESEM instrument (JSM-6701F). The surface area and pore size distribution of the samples were confirmed using Brunauer-Emmett-Teller (BET) and Barrett-Joyner-Halenda (BJH) equations from adsorption-desorption isotherms at 77 K obtained by using 3Flex Surface Characterisation Analyser (Micromeritics). Before analysis, all the samples were degassed at 573 K for 4 hours. Temperature programmed reduction (TPR) was conducted to investigate the reducible species of surface vanadia on TiO2. Selected samples were analysed in the temperature range of 573-973 K on Micromeritics AutoChem II 2920 chemisorption analyser. Prior to measurement, the samples were pre-treated under N2 gas flowing at 473 K for 15 minutes. Argon gas, which contained 5.1% H<sub>2</sub>, was passed through the sample tube during measurement with the flow rate of 25 cm<sup>3</sup>/min. Zeta potential of the samples was recorded on Malvern Zetasizer Nano ZSP.

# Adsorption and photocatalytic degradation

Adsorption and photocatalytic testing were carried out on all synthesised materials. Aqueous solution of 50 mL 100 ppm MB solution and 0.1 g of the prepared material were placed in a beaker. Adsorption test was conducted prior to photocatalytic evaluation. The mixture was stirred in the dark at a constant temperature for 24 hours for the determination of adsorption capacity. Aliquots of 2 mL were withdrawn at different times within 24 hours and were put through a syringe filter. For the photocatalytic activity evaluation, the sample and MB solution were irradiated by a halogen fibre optic light illuminator (Dolan-Jenner MI 157, 150 W) as the visible light source for 24 hours, straight after the adsorption test of 24 hours. A UV cut-off filter (400 nm, Edmund Optics) was used to filter the UV light. The photocatalytic activity of the samples was assessed using UV-Vis spectrophotometer (Thermo Fisher, Genesys 10S) to measure the concentration of MB solution before and after the photodegradation. Adsorption and photocatalytic activities of undoped TiO<sub>2</sub> and bulk V<sub>2</sub>O<sub>5</sub> were also included for comparison.

### **Results and Discussion**

# **Phases formation**

As evidenced by XRD analysis (Figure 1), the undoped TiO<sub>2</sub> was in pure anatase phase, as its XRD pattern was well-matched with that reported in JCPDS 21-1272. The anatase phase remained after doping of 1 mol% V in 1V-TiO<sub>2</sub>, but the peak becomes slightly broader. The crystallite sizes of the samples were calculated using the Scherrer equation, and the results are shown in Table 1. The crystallite size decreased with an increasing amount of V oxide modifier, suggesting the addition V oxide inhibited the crystal growth of TiO2. As observed, the rutile phase was detected when 2 mol% and above of V oxide was added into TiO2, indicating the presence of an adequate amount of V has induced transformation of anatase to rutile phase. It was documented that due to the similar ionic radii of  $V^{4+}(0.580 \text{ Å})$  and  $V^{5+}(0.540 \text{ Å})$ to that of Ti<sup>4+</sup> (0.605 Å) [18], making substitution of Ti by V at substitutional position possible. Therefore, it resulted in rutile phase formation [19]. The result was in good agreement with the previous study, which stated that the formation of the rutile phase upon V doping [20]. The detection of rutile phase was a good indication of successful V incorporated in the TiO2 lattice, even though peaks assigned to V oxides were not detected in all the V-doped TiO<sub>2</sub> samples.

The undetectable V peaks could be attributed to a little amount of the V dopant (at low concentration of V dopant), or the dopant was highly dispersed on the  $TiO_2$  surface. Alternatively, the undetectable vanadia peak was ascribed to amorphous nature of vanadia [21]. XRD pattern of the bulk  $V_2O_5$  was in agreement with the reported pattern (JCPDS 01-0359), indicating it crystallised in orthorhombic structure. The current study indicated that the vanadium oxide present in the current sample was crystalline, not amorphous.

The percentage of anatase phase in the synthesized V-doped TiO<sub>2</sub> samples was calculated using the Spurr equation [22]:

$$A (\%) = 100 / (1 + 1.265 I_R/I_A)$$
 (1)

where  $I_R$  is intensity of rutile peak at  $2\theta = 27.5^{\circ}$  (110) and  $I_A$  is intensity of anatase peak at  $2\theta = 25.5^{\circ}$  (101).

The percentage of rutile phase was obtained via subtraction of 100% on the calculated anatase percentage, assuming that the materials were totally crystallised.

Table 1 lists the anatase and rutile percentages in the synthesised samples. It was found that the percentage of rutile phase was independent to the amount of V dopant and remained constant in the range of 20.0% to 23.6%. The anatase to rutile transformation can be explained in terms of the valency state of the ion. Every four doping of V<sup>5+</sup> in the Ti<sup>4+</sup> octahedral cationic site led to one Ti<sup>4+</sup> cation vacancy, which promotes the rutile phase formation. However, as the V amount increased, the accommodation of excess cation vacancy seems unfavourable in the anatase structure [23]. Hence, further addition of V oxide modifier did not promote more anatase-rutile transformation.

# **Optical properties**

The prepared TiO<sub>2</sub> was a white powdered material, while the bulk V<sub>2</sub>O<sub>5</sub> was an orange powder. All the V-TiO<sub>2</sub> samples were brownish. The colour of the V-TiO<sub>2</sub> samples was more intense, with the increase of the V content. A similar observation was reported previously [15]. As depicted in Figure 2, the undoped TiO<sub>2</sub> has absorption bands in the UV region ranged from 200-400 nm. The dominant peak found at 330 nm was identified as octahedral Ti species, while the shoulder at 230 nm was associated with tetrahedral coordinated Ti species [24]. Redshifts and new peaks of absorption within a range of 400-800 nm was observed after the modification with V oxides. In the resulting products, the extension in the absorption spectrum was demonstrated by the colour changes. The tailing of absorption curves revealed that all the V-TiO<sub>2</sub> materials absorbed the photon energy in the visible light region ranged 380-780 nm. The broadened peaks at 570 and 770 nm were due to  $V^{5+}$  and  $V^{4+}$ , respectively [25]. As can be seen, the intensity of the V<sup>5+</sup> absorption peak increased with the increase of V content in the samples. The 10V-TiO<sub>2</sub> sample possessed the highest amount of V<sup>5+</sup>, followed by 4V-TiO<sub>2</sub>, 3V-TiO<sub>2</sub>, 2V-TiO<sub>2</sub>, and 1V-TiO<sub>2</sub>. For bulk V<sub>2</sub>O<sub>5</sub>, the presence of a shoulder at 242 nm and two peaks at 380 and 480 nm were due to transitions in ligand-metal charge transfer (LMCT)

involving the charge transfer from oxygen ligands to the  $V^{5+}$  metal cation [26].

The bandgap energy of the samples was calculated from the Tauc plot. The following equation was used:  $\alpha hv =$  $A(h\nu-E_g)^{n/2}$ , where  $\alpha$ ,  $h\nu$ , A,  $E_g$  are absorption coefficient, photon energy, a constant, and an optical bandgap, respectively. In this equation, n is determined by the transition type; n value is 1 and 4, for direct and indirect bandgap transitions. The value of n and Eg were first determined by plotting the graph  $In(\alpha h v)$  vs.  $In(h v - \alpha h v)$ E<sub>g</sub>), using an appropriate value of E<sub>g</sub>. The value of n was determined from the slope of the straight line near the band edge. After that,  $(\alpha h \nu)^{2/n}$  vs.  $h \nu$  was formed, and a tangential line was plotted along the band edge, with the tangent line x-intercept corresponding to the optical bandgap. The obtained results are tabulated in Table 1. The findings showed that the bandgap energy of TiO<sub>2</sub> (3.25 eV) dropped significantly after doping of 1 mol% V into TiO<sub>2</sub> (2.15 eV). The bandgap energy of TiO<sub>2</sub> was further decreased with increasing of V amount. It was believed that the 3d orbital of vanadia had reduced the bandgap energy of TiO<sub>2</sub>. The lowest bandgap energy of 1.50 eV was achieved in 10V-TiO<sub>2</sub>.

### Morphology

FESEM images of undoped  $TiO_2$  and selected V- $TiO_2$  samples are illustrated in Figure 3. Undoped  $TiO_2$  (Figure 3(a)) appeared to be large blocks of coarse material. The addition of 1 mol% V dopant also displayed similar features to undoped  $TiO_2$ , but with the formation of more small particles on the large material. Also, holes are formed between the particles, as shown in Figure 3(b).

Sample 4V-TiO<sub>2</sub> showed more small particles agglomerated with reduced holes between the small particles on the surface of the larger particle course. The surface of 10V-TiO<sub>2</sub> sample was smoother and more homogeneous, with small spherical particles agglomerated on the surface of TiO<sub>2</sub>. The current results revealed that the addition of V oxide modifier could alter the morphology of undoped TiO<sub>2</sub> powder to be smoother. The FESEM images of V-TiO<sub>2</sub> supported the XRD results whereby the addition of excess V dopants (> 2 mol%) was not favourable in the anatase structure

and could have resided on the surface of  $\text{TiO}_2$  to form  $V_2O_5$ .

### **Textural analysis**

The nitrogen adsorption-desorption isotherms of samples are presented in Figure 4. All synthesised samples possessed type IV isotherm, which is the characteristic of a mesoporous material. From the isotherm curve, it was observed that undoped TiO<sub>2</sub>, 1V-TiO<sub>2</sub>, and 2V-TiO<sub>2</sub> have H3 hysteresis loops, indicating the samples have slit-shaped pores. As the amount of V dopant increased, the hysteresis loops changed from H3 to H2 for samples 3V-TiO2 and 4V-TiO2, indicating these samples have bottleneck shape pore. Meanwhile, 10V-TiO<sub>2</sub> has hysteresis loop of H1, denoting the pore shape was cylinder-shaped. It was observed that the closing of the hysteresis loop of samples 1 to 4 mol% V-TiO<sub>2</sub> was approximately at 0.45 P/P<sub>o</sub>, while the closing loop of 10V-TiO<sub>2</sub> was at 0.75 P/P<sub>o</sub>. The results suggested that former samples had smaller mesopores while the latter sample had larger mesopores. In addition, 10V-TiO<sub>2</sub> possessed macropores since it showed a slight increase in adsorption in 0.95-1.00 P/P<sub>o</sub>.

The specific surface area, total pore volume, and average pore diameter of samples are tabulated in Table 2. The increasing amount of V oxide modifier increased the surface area of TiO<sub>2</sub> by 2-fold from 17 to 34 m<sup>2</sup> g<sup>-1</sup>. The increase of the surface area could be ascribed to the presence of V, which inhibited the crystalline growth, leading to an enlarged surface area. However, the addition of 10 mol% V reduced the surface area to 23 m<sup>2</sup> g<sup>-1</sup>. This was due to the excess modifier covering the surface of TiO<sub>2</sub>, as demonstrated by Figure 3(d). It is evident from Figure 3(d) that the surface of 10V-TiO<sub>2</sub> had been covered up by the modifier compared to Figure 3(a), which depicts the TiO<sub>2</sub> without a modifier.

Addition of 1 to 3 mol% V has a negligible effect on the total pore volume. The increase of pore volume for 4V-TiO<sub>2</sub> and 10V-TiO<sub>2</sub> samples was in agreement with the changing of the hysteresis loop, whereby the hysteresis loop H2 of 4V-TiO<sub>2</sub> was larger as compared to 3V-TiO<sub>2</sub> sample. Meanwhile, 10V-TiO<sub>2</sub> has the most significant total pore volume among the samples because it

possessed macropores as evidenced by the isotherm plot.

The BJH pore size distribution is shown in Figure 5. The pore size was tuneable with the addition of V oxide modifier. The pore size distribution of samples with less than 4 mol% V became more homogenous and shifted to smaller pore size.

The current result is supported by the FESEM images where the pores between particles (textural) were reduced. The average pore diameter of  $10V\text{-TiO}_2$  was the largest among the samples. Figure 5 shows that  $10V\text{-TiO}_2$  has pores larger than 50 nm, confirming that this sample consisted of a mixture of meso and macropores, leading to the largest average pore diameter.

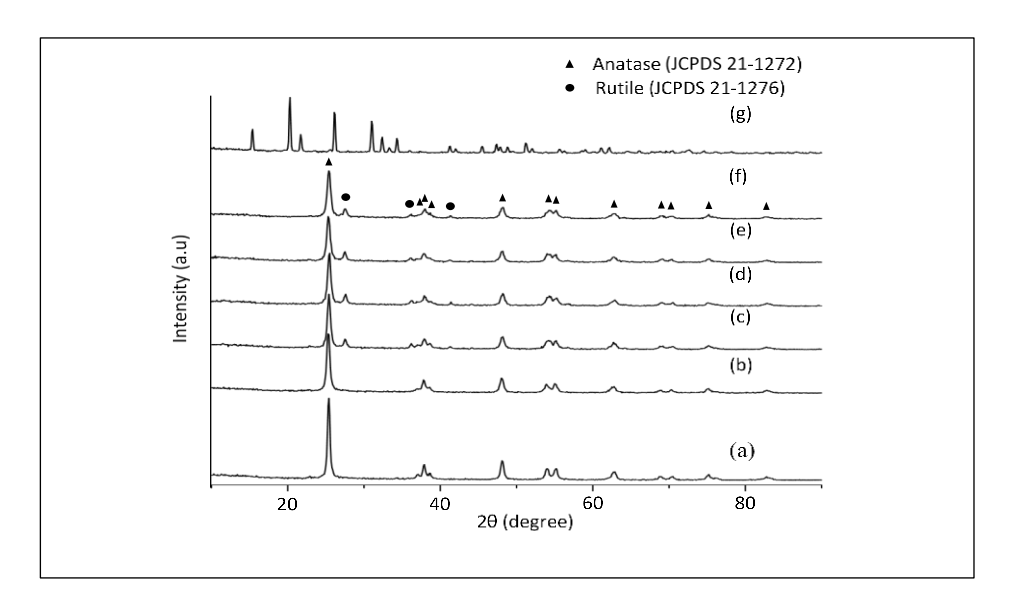


Figure 1. XRD patterns of (a) TiO<sub>2</sub>, (b) 1V-TiO<sub>2</sub>, (c) 2V-TiO<sub>2</sub>, (d) 3V-TiO<sub>2</sub>, (e) 4V-TiO<sub>2</sub>, (f) 10V-TiO<sub>2</sub>, and (g) V<sub>2</sub>O<sub>5</sub>

Table 1.	Phases composition,	crystallite size and	bandgap energy of	TiO <sub>2</sub> , \	$V_2O_5$ and '	V-TiO <sub>2</sub> samples
----------	---------------------	----------------------	-------------------	----------------------	----------------	----------------------------

Sample	Anatase (%) <sup>a</sup>	Rutile (%)b	Crystallite size (nm)	Bandgap (eV) <sup>c</sup>
TiO <sub>2</sub>	100.0	n.a.	20.1	3.25
1V-TiO <sub>2</sub>	100.0	n.a.	16.2	2.75
2V-TiO <sub>2</sub>	80.0	20.0	16.5	2.00
3V-TiO <sub>2</sub>	77.4	22.6	14.7	1.95
4V-TiO <sub>2</sub>	76.4	23.6	14.8	1.80
10V-TiO <sub>2</sub>	78.2	21.8	14.5	1.50
$V_2O_5$	n.a	n.a	n.a	2.30

<sup>&</sup>lt;sup>a</sup> Calculated from Spurr equation, <sup>b</sup> Calculated from 100%- anatase phase%, <sup>c</sup> Calculated from extrapolation of Tauc plot and n.a. – not available

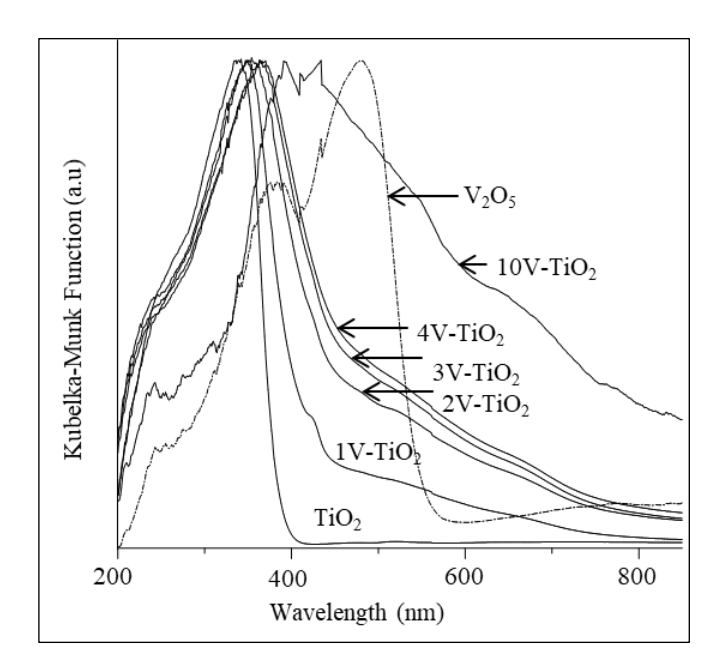


Figure 2. DR-UV-Vis spectra of TiO<sub>2</sub>, V<sub>2</sub>O<sub>5</sub>, and V-doped TiO<sub>2</sub> samples

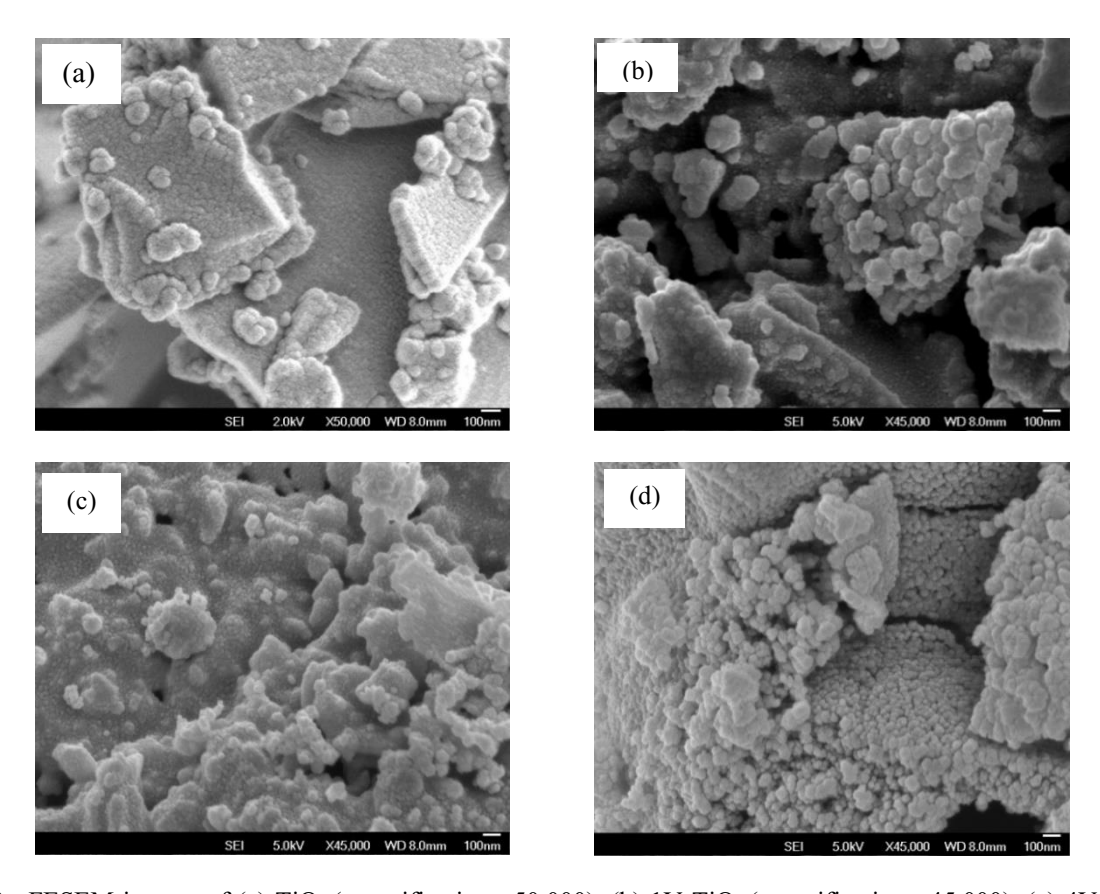


Figure 3. FESEM images of (a)  $TiO_2$  (magnification  $\times 50,000$ ), (b)  $1V-TiO_2$  (magnification  $\times 45,000$ ), (c)  $4V-TiO_2$  (magnification  $\times 45,000$ ), and (d)  $10V-TiO_2$  (magnification  $\times 45,000$ )

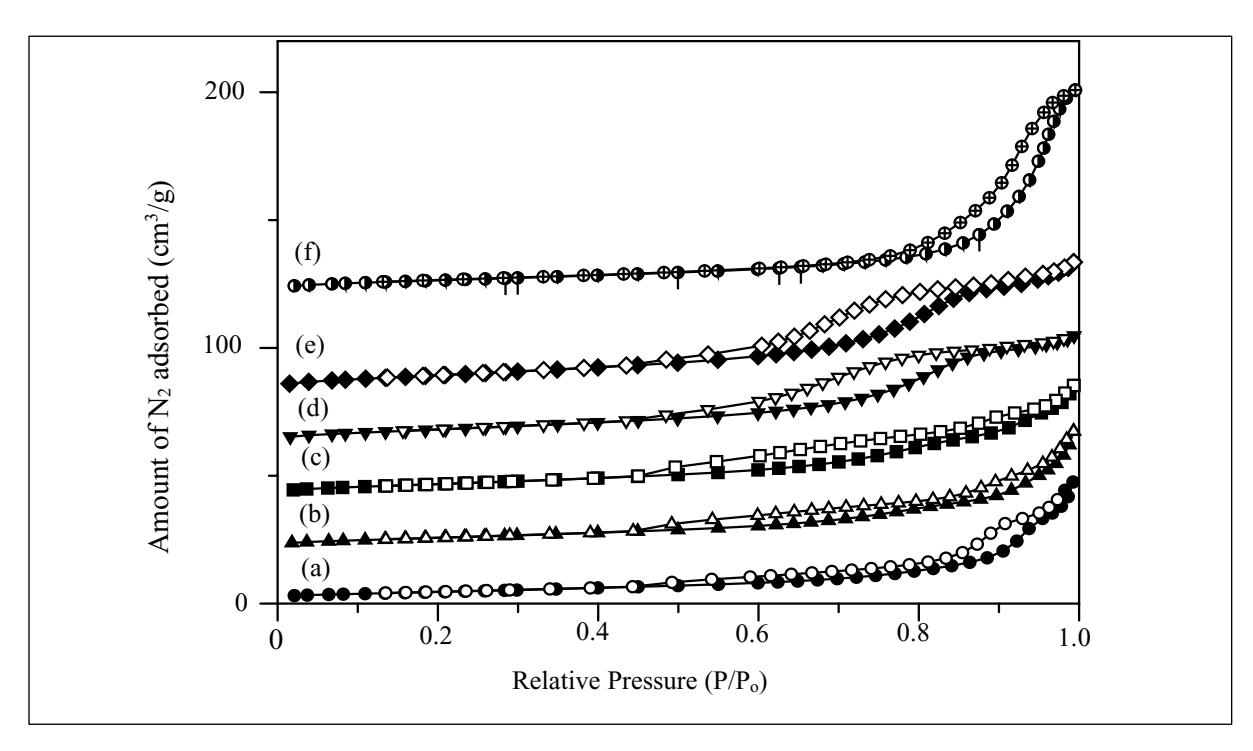


Figure 4. N<sub>2</sub> adsorption-desorption isotherms of (a) TiO<sub>2</sub>, (b) 1V-TiO<sub>2</sub>, (c) 2V-TiO<sub>2</sub>, (d) 3V-TiO<sub>2</sub>, (e) 4V-TiO<sub>2</sub>, and (f) 10V-TiO<sub>2</sub>. (Remarks: filled points are adsorption isotherms, empty points are desorption isotherms. Figures (b)–(f) are marginally moved upwards for 20, 40, 60, 80, and 120 cm<sup>3</sup>/g, respectively for clearer presentation).

Table 2. Surface area, total pore volume and average pore diameter of TiO2 and V-TiO2 samples

Sample	Surface Area (m² g-¹)	Total Pore Volume (cm <sup>3</sup> g <sup>-1</sup> )	Average Pore Diameter (Å)
TiO <sub>2</sub>	17	0.0677	164.27
1V-TiO <sub>2</sub>	21	0.0659	125.94
2V-TiO <sub>2</sub>	25	0.0649	105.38
3V-TiO <sub>2</sub>	29	0.0660	90.12
4V-TiO <sub>2</sub>	34	0.0794	94.78
10V-TiO <sub>2</sub>	23	0.1218	212.00

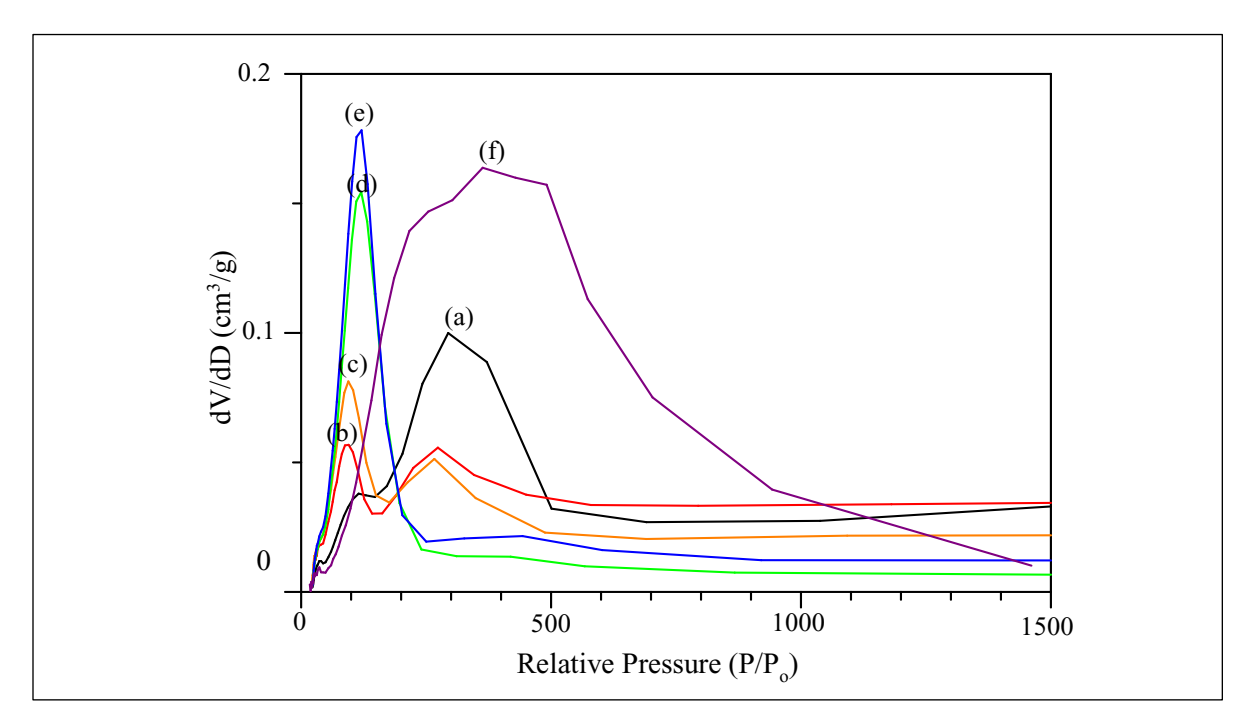


Figure 5. BJH pore size distributions of (a) TiO<sub>2</sub>, (b) 1V-TiO<sub>2</sub>, (c) 2V-TiO<sub>2</sub>, (d) 3V-TiO<sub>2</sub>, (e) 4V-TiO<sub>2</sub>, and (f) 10V-TiO<sub>2</sub>

# Surface oxidation state analysis

Temperature program reduction (TPR) was performed on selected samples to analyse vanadium surface oxidation states in the samples. H2-TPR spectra of V-TiO<sub>2</sub> samples and V<sub>2</sub>O<sub>5</sub> are shown in Figure 6. The 1 mol% V gave only one reduction peak at 814.3 K, which corresponded to the reduction of V<sub>6</sub>O<sub>13</sub> to V<sub>2</sub>O<sub>4</sub> [27], indicating that V<sup>4+</sup> existed dominantly in 1V-TiO<sub>2</sub>. The higher amount of V oxide modifier (4 mol%) resulted in a lower reduction peak at 647.4 K in 4V-TiO<sub>2</sub>. This peak was associated with the reduction of  $V_2O_5$  to  $V_6O_{13}$  [27]; hence, it was a good indication of V<sup>5+</sup> species existence. The detection of this peak is always linked to the formation of the strong interaction between V species and the H<sub>2</sub> gas due to V-O-Ti bonds of higher reducibility. Besides, a hump at 765.1 K was also observed in 4V-TiO<sub>2</sub>, implying the presence of trace V<sup>4+</sup> species.

Similarly, 10V-TiO<sub>2</sub> exhibited two reduction peaks at 684.5 and 841.3 K. Figure 6 shows that the intensity of the reduction peak at 684.5 K is remarkably higher than that of 4V-TiO<sub>2</sub>, strongly indicating the existence of more V<sup>5+</sup> in 10V-TiO<sub>2</sub> compared to the latter sample. The maximum reduction temperature and the corresponded hydrogen consumption of each sample are tabulated in Table 3. As observed, the amount of V<sup>5+</sup> in the 10V-TiO<sub>2</sub> was 5-fold of that in 4V-TiO<sub>2</sub>. The bulk V<sub>2</sub>O<sub>5</sub> showed only one reduction peak at 867.6 K, which corresponded to bulk vanadate. It was reported that more bulk vanadate was formed with increasing of vanadia content in vanadia-titania catalyst [27].

The contradiction could be due to different synthetic method and calcination temperature applied in the studies. The authors had synthesised vanadia-titania via the impregnation method at 673 K. Unlike the impregnation method, the sol-gel method applied in the current work was believed to enable the loading of vanadia not only on the TiO<sub>2</sub>'s surface but also in the

 $TiO_2$  lattice. Meanwhile, the higher calcination temperature of 773 K had resulted in more interaction between vanadia and  $TiO_2$  that facilitated the formation of more reducible  $V^{5+}$  species in the materials [28]. In the present work, the decrease of reduction temperature in  $V_2O_5$  in the presence of  $TiO_2$  can be explained by the structure distortion in  $V_2O_5$  due to the extensive interaction with the  $TiO_2$  support. A similar phenomenon was found for 12-molybdophosphoric acid supported on  $V_2O_5$  dispersed  $\gamma$ -Al $_2O_3$  catalyst [29]. Therefore, we conclude that the presence of  $TiO_2$  phase is essential as support for  $V^{5+}$  species formation.

# Adsorption and photocatalytic performance

Adsorption and photocatalytic activity of the resulting V-TiO<sub>2</sub> samples were assessed over decolourisation of MB. As illustrated in Figure 7, the adsorption of MB on undoped TiO<sub>2</sub> is only 3% after 24 hours. Doping of 1 mol% V into TiO<sub>2</sub> allows 1V-TiO<sub>2</sub> to adsorb 9% MB after 2 hours. The increased V dopant amount of 2, 3, 4, and 10 mol% V had further enhanced the MB adsorption to 18%, 25%, 31%, and 68% after 2 hours. The adsorption of MB increased significantly by the increasing amount of V in V-TiO<sub>2</sub>. The results demonstrated that the adsorption capacity of 10V-TiO<sub>2</sub> was 26-folds higher than that of undoped TiO<sub>2</sub>. This material adsorbed 95% MB after 24 hours, confirming it was an excellent adsorbent for MB.

Zeta potential was conducted to analyse the surface charge of the samples. It was found that the increased amount of V oxide modifier to 10 mol% decreases the isoelectric point (IEP) continuously from 4.23 to 2.01 (Table 3). This could be the reason for the tremendous increase of MB adsorption, a cationic dye, up to 68% after 2 hours when TiO2 was modified with 10 mol% V oxide. In addition, MB has a high affinity for V<sup>5+</sup> [30]. This further enhanced the adsorption capacity of MB on 10V-TiO<sub>2</sub>, which possessed the highest amount of V<sup>5+</sup> among the samples. Comparatively, the adsorption ability of the bulk V<sub>2</sub>O<sub>5</sub> was poorer as it adsorbed only 40% of MB after 2 hours. The lower activity of bulk V<sub>2</sub>O<sub>5</sub> could be attributed to its massive structure which makes the accessibility of MB on V5+ more difficult. Besides, the superior adsorption capability of 10V-TiO<sub>2</sub> as compared to bulk V<sub>2</sub>O<sub>5</sub> could be due to the existence of more surface  $OH^-$  in  $10V-TiO_2$  to interact with the  $\pi$ -electron of MB [16, 31].

The photocatalytic activity evaluation was carried out straight after the adsorption test with the samples. Figure 7 displays that the undoped TiO<sub>2</sub> gave an activity of 14.4% of MB photodegradation even with the utilisation of UV cut-off filter (400 nm, Edmund Optics). This can be rationalised by the photosensitisation effect [32]. Usage of MB as a model reaction in photocatalysis has been highlighted by Ohtani and co-worker [33]. The authors claimed that MB was not an acceptable pollutant for the target study, particularly when it was degraded under visible light. However, Matos et al. [34] argued that the decolourisation of MB is suitable for assessing the photocatalytic behaviour of semiconductors under steady-state conditions of the effect of photon flux upon the first-order rate constant.

Among the V-TiO<sub>2</sub> samples, only the 4V-TiO<sub>2</sub> sample has photodegraded 13.5% of MB after 24 hours under visible light irradiation. The other V-TiO<sub>2</sub> samples have negligible photocatalytic activity under visible light irradiation. In contrast, it had been documented that photocatalytic activity TiO2 in dye degradation was significantly enhanced after V doping [35]. The photocatalytic improvement was always associated with the extended optical absorption of TiO2 to the visible light, reduction in bandgap energy and the presence of anatase/rutile mixing phase. In the present study, the MB molecules were preferably adsorbed at the V site due to the high affinity of V5+. The strong interaction between V5+ and the MB molecules was believed to hinder the diffusion of the dye molecules to the active site for photodegradation at Ti; hence, retard the photocatalytic activity of the V-doped TiO<sub>2</sub> samples. In 4V-TiO<sub>2</sub>, only limited MB molecules that adsorbed at Ti site would be further photodegraded after irradiated under visible light. The schematic diagram showing roles of the vanadia and titania phases in the dye removal is illustrated in Figure 8.

Even though the photocatalytic activity of the  $V\text{-}TiO_2$  was not comparable to its adsorption ability, the total removal of MB of  $V\text{-}TiO_2$  significantly increased as compared to  $TiO_2$  and  $V_2O_5$ . As mentioned, the

photocatalytic enhancement of TiO2 was always related to the extension of optical absorption to the visible light region. By comparing the adsorption and photocatalytic testing of V-TiO<sub>2</sub> samples to the XRD results as represented in Figure 1 and Table 1, it can be seen that part of the anatase to rutile phase transformation induced by the doping of V into TiO2 might have enhanced the photodegradation of MB to visible light region, attributed by the lower bandgap energy (3.0 eV) of the rutile phase as compared to the anatase phase (3.2 eV). It is suggested in this study that the vanadia and titania played a different role in the adsorption-photocatalytic activity. The vanadia responsible for the anatase to rutile phase transformation as well as the shifting of the absorption properties of TiO2 to visible light region, and at the same time, acted as an adsorbent, while the titania acted as the photocatalyst, responsible for the photodegradation activity.

# Reusability test

Since 10V-TiO<sub>2</sub> has the highest removal of MB, it was chosen for the reusability test. The used 10V-TiO<sub>2</sub> was washed with distilled water several times and dried at

333 K. The reusability test was conducted for four successive cycles under the same conditions. It was found out that the adsorption capacity of the used-10V-TiO<sub>2</sub> decreased significantly to 28%, 26%, and 27% for second, third, and fourth cycles, respectively. The decrease of the adsorption capacity could be attributed to the leaching problem of vanadium oxide from the material. It was believed that the loss of the vanadium oxide could have decreased the hydroxyl surface group and hence leading to less adsorption of MB [36]. It was noted that after the adsorption for the first cycle, the adsorption for the rest of the cycles was almost constant, indicating that the material has become stable. It is worth to highlight that the photocatalytic performance of 10V-TiO<sub>2</sub> increased to approximately 30% for the second, third, and fourth cycles (Figure 9). The improvement in photocatalytic performance could be attributed to more TiO<sub>2</sub> were exposed to MB, leading to a more significant degradation of MB. The study indicated that 10V-TiO<sub>2</sub> was a good photocatalyst for MB photodegradation after second cycles onwards.

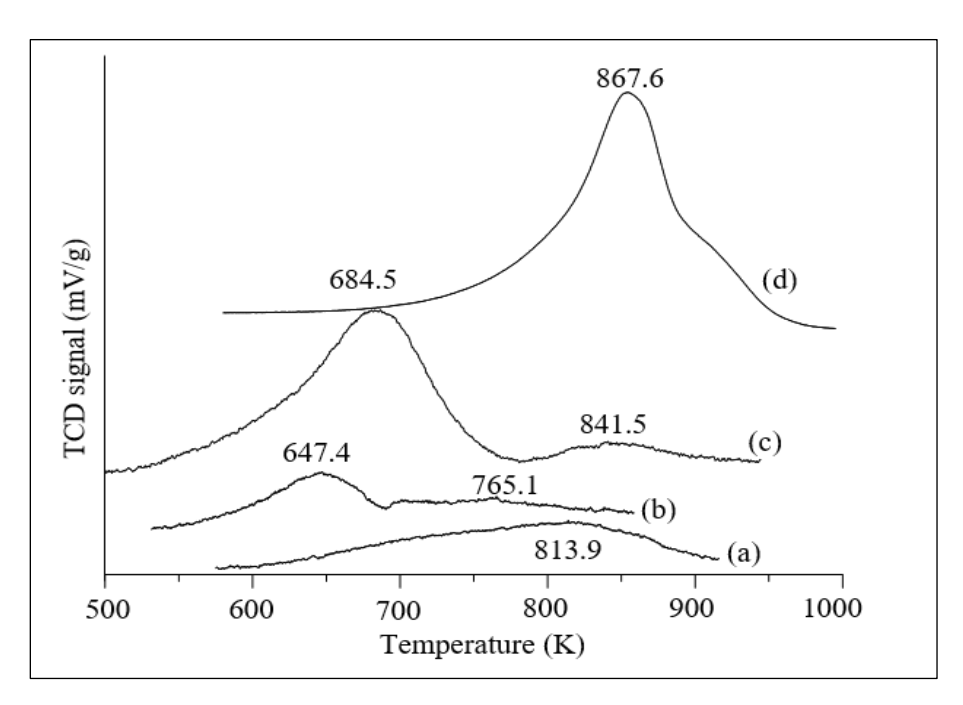


Figure 6. TPR profiles of (a)1V-TiO<sub>2</sub>, (b) 4V-TiO<sub>2</sub>, (c) 10V-TiO<sub>2</sub>, (d) V<sub>2</sub>O<sub>5</sub> (Intensity of V<sub>2</sub>O<sub>5</sub> is multiplied with 0.1)

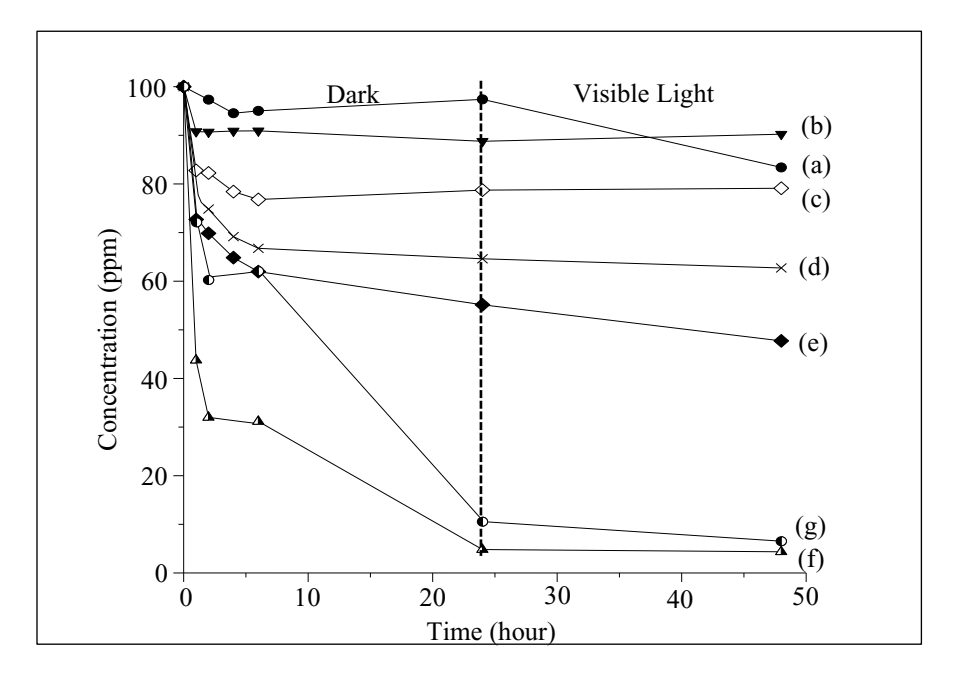


Figure 7. The adsorption and photodegradation of MB using (a)  $TiO_2$ , (b)  $1V-TiO_2$ , (c)  $2V-TiO_2$ , (d)  $3V-TiO_2$ , (e)  $4V-TiO_2$ , (f)  $10V-TiO_2$ , (g)  $V_2O_5$ 

Table 3. Isoelectric point of prepared samples and its corresponded adsorption efficiency after 2 hours

Entry	Sample	IEP/pH	Adsorption Efficiency After 2 hours /%
1	TiO <sub>2</sub>	4.23	3
2	1V-TiO <sub>2</sub>	4.14	9
3	2V-TiO <sub>2</sub>	4.13	18
4	3V-TiO <sub>2</sub>	4.12	25
5	4V-TiO <sub>2</sub>	2.22	31
6	10V-TiO <sub>2</sub>	2.01	68

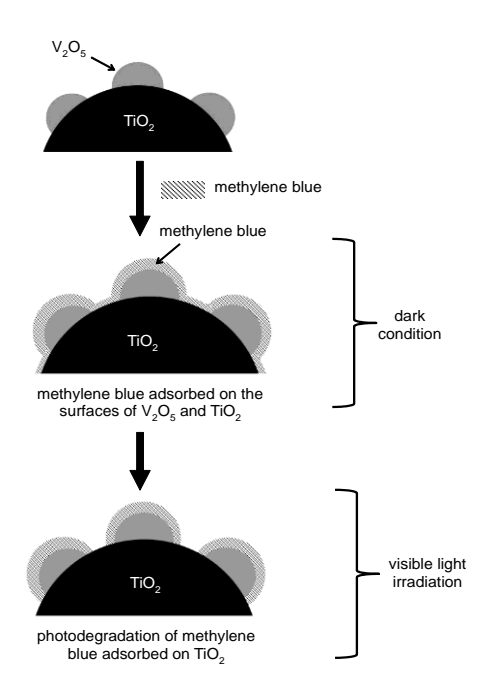


Figure 8. Schematic diagram showing the roles of vanadia and titania

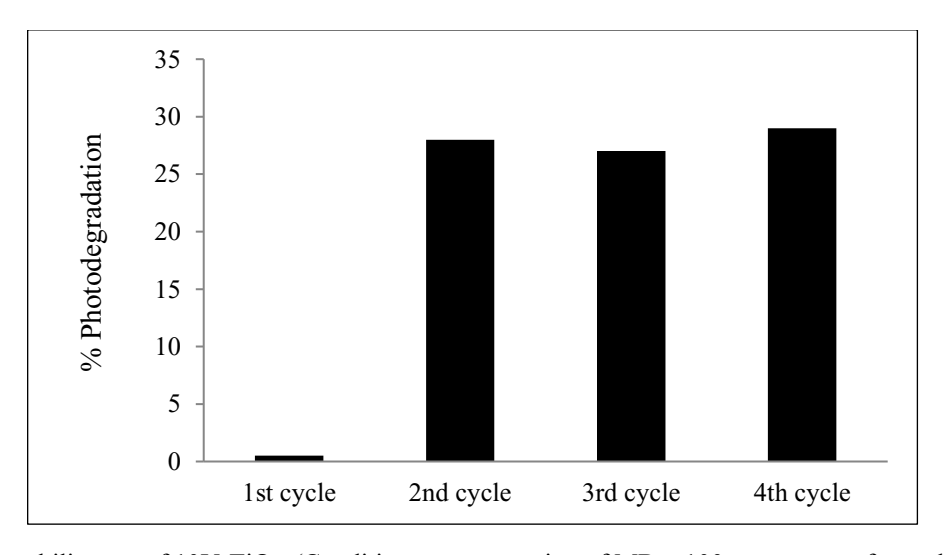


Figure 9. Reusability test of 10V-TiO<sub>2</sub>. (Conditions: concentration of MB = 100 ppm, mass of sample used = 0.1 g)

# Conclusion

A series of V modified TiO<sub>2</sub> was successfully synthesised *via* the sol-gel method. Roles of vanadia and titania phases in the removal of MB were examined. The results demonstrated that the presence of vanadia phase was responsible for the rutile phase generation, bandgap

reduction, and wavelength extension in the V-TiO<sub>2</sub> samples. On the other hand, the titania phase played a crucial role as support for the formation of more  $V^{5+}$  species. In the V oxide modified TiO<sub>2</sub> materials, vanadia phase was an excellent adsorbent attributed to the presence of  $V^{5+}$  species is abundant, which has a high

affinity towards MB. Meanwhile, the titania phase acted as the photocatalyst in degrading MB.  $10V\text{-TiO}_2$  showed high photostability and reusability in photodegrading MB in second cycles and onward, attributed to more exposed of  $\text{TiO}_2$  to MB.

# Acknowledgement

Authors are grateful to financial support from Ministry of Higher Education Malaysia (MOHE) and Universiti Teknologi Malaysia through UTM Transdisciplinary Research Grant (Cost Centre No. Q.J130000.3554.07G57) and Professional Development Research University (Cost Centre No. Q.J.130000.21A2.03E61).

#### References

- Koh, P. W., Yuliati, L. and Lee, S. L. (2019). Kinetics and optimization studies of photocatalytic degradation of methylene blue over Cr-doped TiO<sub>2</sub> using response surface methodology. *Iranian Journal of Science and Technology, Transactions A: Science*, 43(1): 95-103.
- 2. Koh, P. W., Hatta, M. H. M., Ong, S. T., Yuliati, L. and Lee, S. L. (2017). Photocatalytic degradation of photosensitizing and non-photosensitizing dyes over chromium doped titania photocatalysts under visible light. *Journal of Photochemistry and Photobiology A: Chemistry*, 332: 215-223.
- 3. Kumar, P. S., Ramalingam, S. and Sathishkumar, K. (2011). Removal of methylene blue dye from aqueous solution by activated carbon prepared from cashew nut shell as a new low-cost adsorbent. *Korean Journal of Chemical Engineering*, 28(1): 149-155.
- Roosta, M., Ghaedi, M., Daneshfar, A., Sahraei, R. and Asghari, A. (2014). Optimization of the ultrasonic assisted removal of methylene blue by gold nanoparticles loaded on activated carbon using experimental design methodology. *Ultrasonics Sonochemistry*, 21(1): 242-252.
- Keng, P. S., Lee, S. L., Ha, S. T., Hung, Y. T. and Ong, S. T. (2013). Cheap materials to clean heavy metal polluted waters. In Green Materials for Energy, Products and Depollution Springer, Dordrecht: pp. 335-414.

- 6. Leong, C.Y., Koh, P.W., Lo, Y.S., Lee, S.L. (2020). Hydrothermal synthesis of titanium dioxide nanotube with methylamine for photodegradation of Congo red. *IOP Conf. Series: Materials Science and Engineering*, 833, 012075.
- 7. Pirkanniemi, K. and Sillanpää, M. (2002). Heterogeneous water phase catalysis as an environmental application: a review *Chemosphere*, 48(10): 1047-1060.
- MiarAlipour, S., Friedmann, D., Scott, J. and Amal, R. (2018). TiO<sub>2</sub>/porous adsorbents: Recent advances and novel applications. *Journal of Hazardous Materials*, 341: 404-423.
- 9. Ooi, Y. K., Hussin, F., Yuliati, L. and Lee, S. L. (2019). Comparison study on molybdena-titania supported on TUD-1 and TUD-C synthesized via sol-gel templating method: Properties and catalytic performance in olefins epoxidation. *Materials Research Express*, 6(7): 074001.
- Ooi, Y. K., Yuliati, L., Hartanto, D., Nur, H. and Lee, S. L. (2016). Mesostructured TUD-C supported molybdena doped titania as high selective oxidative catalyst for olefins epoxidation at ambient condition. *Microporous and Mesoporous Materials*, 225: 411-420.
- 11. Wang, N., Zhu, L. H., Li, J., and Tang, H. Q. (2007). A novel Fe(OH)<sub>3</sub>/TiO<sub>2</sub> nanoparticles and its high photocatalytic activity. *Chinese Chemical Letters*, 18(10): 1261-1264.
- 12. Hamdan, H., Muhid, M. N. M., Lee, S. L., and Tan, Y. Y. (2009). Visible light enabled V and Cr doped titania-silica aerogel photocatalyst. *International Journal of Chemical Reactor Engineering*, 7(1).
- 13. Ooi, Y. K., Yuliati, L., and Lee, S. L. (2016). Phenol photocatalytic degradation over mesoporous TUD-1-supported chromium oxide-doped titania photocatalyst. *Chinese Journal of Catalysis*, 37(11): 1871-1881.
- 14. Wu, J. C. S. and Chen, C. H. (2004). A visible-light response vanadium-doped titania nanocatalyst by sol–gel method. *Journal of Photochemistry and Photobiology A: Chemistry*, 163(3): 509-515.

- 15. Li, H., Zhao, G., Chen, Z., Han, G. and Song, B. (2010). Low temperature synthesis of visible light-driven vanadium doped titania photocatalyst. *Journal of Colloid and Interface Science*, 344(2): 247-250.
- Nguyen, T. B., Hwang, M. J., and Ryu, K. S. (2012). High adsorption capacity of V-doped TiO<sub>2</sub> for decolorization of methylene blue. *Applied Surface Science*, 258(19): 7299-7305.
- 17. Koh, P. W., Yuliati, L., and Lee, S. L. (2014). Effect of transition metal oxide doping (Cr, Co, V) in the photocatalytic activity of TiO<sub>2</sub> for congo red degradation under visible light. *Jurnal Teknologi* (Sciences & Engineering), 69(5): 45-50.
- 18. Shannon, R. D. (1976). Revised effective ionic radii and systematic studies of interatomic distances in halides and chalcogenides. *Acta Crystallographica Section A: Crystal Physics, Diffraction, Theoretical and General Crystallography*, 32(5): 751-767.
- 19. Choi, J., Park, H. and Hoffmann, M. R. (2009). Effects of single metal-ion doping on the visible-light photoreactivity of TiO<sub>2</sub>. *The Journal of Physical Chemistry C*, 114(2): 783-792.
- Martin, S. T., Morrison, C. L., and Hoffmann, M. R. (1994). Photochemical mechanism of size-quantized vanadium-doped TiO<sub>2</sub> particles. *The Journal of Physical Chemistry*, 98(51): 13695-13704.
- Pena, D. A., Uphade, B. S., and Smirniotis, P. G. (2004). TiO<sub>2</sub>-supported metal oxide catalysts for low-temperature selective catalytic reduction of NO with NH<sub>3</sub>: I. Evaluation and characterization of first row transition metals. *Journal of Catalysis*, 221(2), 421-431.
- Spurr, R. A. and Myers, H. (1957). Quantitative analysis of anatase-rutile mixtures with an X-ray diffractometer. *Analytical Chemistry*, 29(5): 760-762.
- 23. Nagaveni, K., Hegde, M. S. and Madras, G. (2004). Structure and photocatalytic activity of  $Ti_{1-x}M_xO_{2\pm\delta}$  (M= W, V, Ce, Zr, Fe, and Cu) synthesized by solution combustion method. *The Journal of Physical Chemistry B*, 108(52): 20204-20212.
- 24. Astorino, E., John, B. Peri, R. J. Willey, and Guido B. (1995). Spectroscopic characterization of

- silicalite-1 and titanium silicalite-1. *Journal of Catalysis*, 157(2): 482-500.
- 25. Bhattacharyya, K., Varma, S., Tripathi, A. K., Bharadwaj, S. R., and Tyagi, A. K. (2008). Effect of vanadia doping and its oxidation state on the photocatalytic activity of TiO<sub>2</sub> for gas-phase oxidation of ethene. *The Journal of Physical Chemistry C*, 112(48): 19102-19112.
- Lewandowska, A. E., Banares, M. A., Khabibulin, D. F. and Lapina, O. B. (2009). Precursor effect on the molecular structure, reactivity, and stability of alumina-supported vanadia. *The Journal of Physical Chemistry C*, 113(48): 20648-20656.
- 27. Shekar, S. C., Soni, K., Bunkar, R., Sharma, M., Singh, B., Suryanarayana, M. V. S., and Vijayaraghavan, R. (2011). Vapor phase catalytic degradation of bis (2-chloroethyl) ether on supported vanadia–titania catalyst. *Applied Catalysis B: Environmental*, 103(1-2): 11-20.
- 28. Olthof, B., Khodakov, A., Bell, A. T. and Iglesia, E. (2000). Effects of support composition and pretreatment conditions on the structure of vanadia dispersed on SiO<sub>2</sub>, Al<sub>2</sub>O<sub>3</sub>, TiO<sub>2</sub>, ZrO<sub>2</sub>, and HfO<sub>2</sub>. *The Journal of Physical Chemistry B*, 104(7): 1516-1528.
- Rao, P. S. N., Rao, K. T. V., Prasad, P. S. S. and Lingaiah, N. (2011). The role of vanadia for the selective oxidation of benzyl alcohol over heteropolymolybdate supported on alumina. *Chinese Journal of Catalysis*, 32(11-12): 1719-1726.
- 30. Zhao, L., Zhu, X., Feng, K., and Wang, B. (2006). Speciation analysis of inorganic vanadium (V(IV)/V (V)) by graphite furnace atomic absorption spectrometry following ion-exchange separation. *International Journal of Environmental and Analytical Chemistry*, 86(12): 931-939.
- 31. Dong, Y., Liu, Y., Lu, D., Zheng, F., Fang, P. and Zhang, H. (2017). Unpredictable adsorption and visible light induced decolorization of nano rutile for the treatment of crystal violet. *Solid State Sciences*, 66: 1-6.

- 32. Yu, L., Yuan, S., Shi, L., Zhao, Y. and Fang, J. (2010). Synthesis of Cu<sup>2+</sup> doped mesoporous titania and investigation of its photocatalytic ability under visible light. *Microporous and Mesoporous Materials*, 134(1-3): 108-114.
- 33. Yan, X., Ohno, T., Nishijima, K., Abe, R. and Ohtani, B. (2006). Is methylene blue an appropriate substrate for a photocatalytic activity test? A study with visible-light responsive titania. *Chemical Physics Letters*, 429(4-6): 606-610.
- 34. Matos, J., Hofman, M. and Pietrzak, R. (2013). Synergy effect in the photocatalytic degradation of

- methylene blue on a suspended mixture of TiO<sub>2</sub> and N-containing carbons. *Carbon*, 54: 460-471.
- 35. Nair, R. G., Roy, J. K., Samdarshi, S. K. and Mukherjee, A. K. (2012). Mixed phase V doped titania shows high photoactivity for disinfection of *Escherichia coli* and detoxification of phenol. *Solar Energy Materials and Solar Cells*, 105: 103-108.
- 36. Wu, H-X, Wang, T-J, Chen, L., Jin, Y., Zhang, Y. and Dou, X-M. (2009). The roles of the surface charge and hydroxyl group on a Fe-Al-Ce adsorbent in fluoride adsorption. *Industrial & Engineering Chemistry Research*, 48(9): 4530-4534.